HHS Public Access

Author manuscript

Cell. Author manuscript; available in PMC 2019 January 11.

Published in final edited form as:

Cell. 2018 January 11; 172(1-2): 262–274.e11. doi:10.1016/j.cell.2017.12.022.

Retrovirus-like Gag protein Arc1 binds RNA and traffics across synaptic boutons

James Ashley[&], **Benjamin Cordy**[&], **Diandra Lucia**, **Lee G Fradkin**, **Vivian Budnik**[*,#], and **Travis Thomson**[*]

Department of Neurobiology, University of Massachusetts Medical School, Worcester MA 01605, USA

Summary

Arc/Arg3.1 is required for synaptic plasticity and cognition and mutations in this gene are linked to autism and schizophrenia. Arc bears a domain resembling retroviral/retrotransposon Gag-like proteins, which multimerize into a capsid that packages viral RNA. The significance of such a domain in a plasticity molecule is uncertain. Here we report that the *Drosophila* Arc1 protein forms capsid-like structures that bind *darc1* mRNA in neurons and is loaded into extracellular vesicles that are transferred from motorneurons to muscles. This loading and transfer depends on the *darc1-mRNA* 3′-untranslated region, which contains retrotransposon-like sequences. Disrupting transfer blocks synaptic plasticity, suggesting that transfer of dArc1 complexed with its mRNA is required for this function. Notably, cultured cells also release extracellular vesicles containing the Gag region of the Copia retrotransposon complexed with its own mRNA. Taken together, our results point to a trans-synaptic mRNA transport mechanism involving retrovirus-like capsids and extracellular vesicles.

In brief

- Retrovirus-like Gag protein Arc1 binds RNA and traffics across synaptic boutons

Corresponding authors: vivian.budnik@umassmed.edu, travis.thomson@umassmed.edu.
[&]These authors contributed equally
[*]Senior authors
[#]Lead contact: Vivian BudnikDepartment of Neurobiology, University of Massachusetts Medical School, LRB 7th floor, 364 Plantation St, Worcester MA 01605

Author contributions (CRediT taxonomy)

Conceptualization: VB and TT; **Methodology**: JA, BC, LF, VB, and TT; **Software**: JA, TT; **Validation**: VB, TT, JA; **Formal Analysis**: TT, JA, VB, BC; **Investigation**: JA, BC, DL, LF and TT; **Resources**: VB, EM core, Neurobiology Department, Deep Sequencing Core; **Data Curation**: TT, JA, VB; **Writing – Original Draft**: VB, TT; **Writing – Review & Editing**: VB, TT, JA, BC, LF; **Visualization**: VB; **Supervision**: VB, JA, TT; **Project Administration**: VB, JA, TT; **Funding Acquisition**: VB.

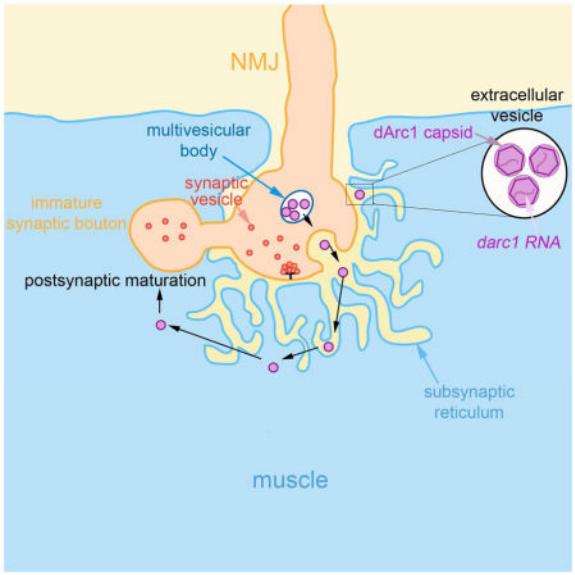

Keywords

Arc/Arg3.1; plasticity; synapse; retrotransposon; exosomes; Gag domain; RNA trafficking; extracellular vesicles; copia; gypsy retrotransposon; trans-synaptic RNA transport; RNA-binding protein

Introduction

Mammalian Activity-Regulated Cytoskeleton-Associated protein (Arc/Arg3.1) is pivotal for synapse maturation, synaptic plasticity, and learning and memory (Shepherd and Bear, 2011). Arc is an activity-dependent immediate early gene, and its mRNA is translocated to dendrites via sequences in its 3′-Untranslated Region (UTR) (Dynes and Steward, 2007). Following plasticity-inducing stimulation *arc* mRNA moves into active dendritic spines, where it is translated and regulates trafficking of AMPA receptors by engaging the endocytic machinery (Chowdhury et al., 2006). Arc is also involved in regulating dendritic spine morphology during plasticity (Peebles et al., 2010). Arc protein is composed of Group-specific antigen (Gag)-like amino acid sequences typically found in retroviruses such as HIV and in retrotransposons (Campillos et al., 2006). Beyond its binding to Tarpγ2, an AMPA-receptor binding protein (Zhang et al., 2015), the physiological significance of the Gag-like sequences in Arc is unknown. During retroviral replication, Gag proteins multimerize into capsids, which bind and package viral RNA (Chen, 2016). Capsids then undergo secondary envelopment by membranes and exit the host cell being competent to infect other cells (Alenquer and Amorim, 2015). There is a growing aggregate of evidence that suggest some viruses, commandeer host exosomal pathways suggesting a connection between viruses and exosomes (Meckes, 2015).

Exosomes and other extracellular vesicles (EVs) such as microvesicles have recently emerged as a novel trans-cellular communication strategy in the healthy and diseased brain (Basso and Bonetto, 2016). For instance, glutamate release by neurons induces

oligodendroglial secretion of exosomes, which are taken up and regulate the physiology of recipient neurons (Fruhbeis et al., 2013). At *Drosophila* neuromuscular synapses, Wnt signaling is mediated by trans-synaptic transfer of the Wnt, Wingless, via exosomes *in vivo* (Koles et al., 2012; Korkut et al., 2009). In mammals, the propagation of neurodegenerative disorders, such as ALS, appears to be partly mediated by the transfer of prion-like proteins across cells via exosomes (Basso and Bonetto, 2016).

In an expression profile of *Drosophila* cultured cell EVs we found that one of the most abundant and enriched mRNAs was the *Drosophila darc1* (also see (Lefebvre et al., 2016). At the NMJ, *darc1* mRNA and protein were enriched at synaptic boutons of the larval NMJ and both were transferred from presynaptic boutons to postsynaptic muscles, likely via EVs. Notably, this transfer was dependent on a *gypsy* retrotransposon-like sequence fragment in the 3′UTR of *darc1*. Evocative of retroviral Gags, dArc1 protein physically associated with its own mRNA. In support of this observation, a spliced fragment of the Copia retrotransposon mRNA and protein were also found within EVs. This retroviral-like mechanism of transfer is required for dArc1 function, as blocking the transfer resulted in aberrations in both synapse maturation and activity-dependent plasticity. We propose that in *Drosophila*, dArc1 influences synaptic plasticity by utilizing a retroviral-like mechanism for transport between synaptic partners.

Results

darc1 mRNA is enriched in S2 cell exosome-like EVs at the *Drosophila* larval NMJ

To elucidate the expression profile of Drosophila S2 cell EVs, we collected EV fractions by differential centrifugation and sucrose gradient sedimentation, treated the EV fraction with RNase to digest non-specifically associated extravesicular cytoplasmic RNA and then constructed poly(A)$^+$ libraries for deep sequencing using RNA collected from treated EVs and total cell mRNA. While most mRNAs in the EV fraction (~96.6% of cellular mRNAs) were equal to or under-represented when compared to total cellular mRNAs, approximately 100 transcripts were enriched in the EV fraction by at least twofold. Among the most abundant and enriched mRNAs was *darc1* (Fig. 1A,B,D). The large enrichment of *darc1* in EV preps was confirmed by qPCR (Fig. 1C). To determine if *darc1* mRNA was present *in vivo* at the *Drosophila* larval NMJ, we conducted fluorescent *in situ* hybridization (FISH) and double labeled the preparation with anti-HRP, an antibody that recognizes neuronal membrane antigens in insects (Jan and Jan, 1982), to label the presynaptic compartment. *darc1 mRNA* was present in a punctate pattern both inside presynaptic boutons and muscles, but was particularly enriched at the muscle postsynaptic junctional region, the region of the muscle immediately adjacent to the HRP label (Fig. 2A). The FISH signal was largely specific since it was severely reduced in a predicted *darc1* null mutant, $darc1^{esm113}$ (Mattaliano et al., 2007), although some residual signal remained (Fig. 2B).

To establish if dArc1 protein was also observed at these sites, we generated a polyclonal anti-dArc1 antibody and found that dArc1 was also present both pre- and postsynaptically at the NMJ, in a pattern very similar to the RNA localization (Fig. 2C). We also generated an independent, cleaner *darc1* null mutant via Crispr/Cas9, $darc1^{E8}$, because the $darc1^{esm113}$ deletion spans into the putative *darc2* promoter region (see methods). In $darc1^{E8}/darc1^{esm113}$

and *darc1*^{wsm113} mutants there was a similar drastic reduction in dArc1 RNA and protein (Fig. 2B,D), but residual signal was still observed. The residual signal might correspond to either maternal contribution of *darc1* RNA, which is quite large, or to unspecific antibody binding. In support to the former possibility, *darc1 RNA* could still be detected in extracts from the mutants by PCR, although the amount was very low compared to wild type (Fig. S1C). The anti-dArc1 antibody recognized a band of the expected molecular weight in Western blots of body wall muscle protein extracts (Fig. 2T) and in immunoprecipitations of dArc1 (Fig. S1A). This band was absent in the *darc1*^{esm113} and *darc1*^{E8}/*darc1*^{esm113} mutant, demonstrating the specificity of the antibody (Fig. 2T;S1A). However, the antibody also recognized higher molecular weight bands (arrow in Fig. 2T) that were not altered by the *darc1* mutation. This indicates that at least some of the residual signal observed in the mutants might be unspecific. Unlike the specific signal, the residual signal was distributed throughout the muscle and was not concentrated at the NMJ. Thus, *darc1* mRNA is enriched in S2 cell EVs, and both *darc1 mRNA* and dArc1 protein are present at pre- and postsynaptic sites of the NMJ.

A postsynaptic muscle *darc1* RNA pool is derived from motorneurons and RNA transfer depends on *darc1* 3′UTR

The ORF of darc1 is mostly represented by the remnant of a Gypsy-superfamily of transposons (Fig. 2U), specifically dArc1 has strong similarities to the GAG region of a Gypsy-like transposon. The presence of *darc1* in EVs together with the observation that *darc1* encodes a retroviral Gag-like protein raised the possibility that the mRNA, similar to retroviral genomic RNA (gRNA), could be transferred across synaptic partners, as we have previously shown for two transmembrane proteins, Evi and Syt4 (Korkut et al., 2009; Korkut et al., 2013). To test this possibility, we downregulated *darc1* exclusively in motorneurons, using the Gal4 driver C380-Gal4 to express UAS-dArc1-RNAi, and examined the pre-and postsynaptic levels of *dArc1* mRNA via FISH. Expressing dArc1-RNAi in motorneurons resulted in a significant decrease in *darc1* FISH signal, not only at presynaptic boutons, but also at the muscle postsynaptic region (Fig. 2E,F,O, Fig. S1B). Given that the C380-Gal4 driver does not express Gal4 in muscles (Budnik et al., 1996) and that we have not previously observed transfer of RNAi between NMJ synaptic partners (e.g., (Ataman et al., 2006)), the most parsimonious explanation is that much of the postsynaptic *darc1* mRNA is derived from a presynaptic pool, presumably via EVs (see Discussion). Similarly to the FISH results, expressing dArc1-RNAi in motorneurons resulted in a significant decrease in dArc1 protein immunoreactive signal, both in pre- and postsynaptic compartments (Fig. 2I,J,P).

In contrast, expressing dArc1-RNAi with a muscle Gal4 driver, C57-Gal4, did not affect *dArc1* RNA nor dArc1 protein levels (Fig. 2H,L,O,P). This raises the possibility that postsynaptic *dArc1* RNA is somehow protected from the RNAi machinery (see Discussion). Taken together, the above results suggest that postsynaptic *darc1* transcript and/or protein is transported from presynaptic boutons to the postsynaptic compartment in a unidirectional manner.

To eliminate the possibility that dArc1 RNAi could, unlike other RNAi species, be transferred from neuron to muscles, we used an approach independent from RNAi to block EV release from presynaptic boutons. We have previously demonstrated that Rab11 is required for the release of exosome-like EVs at the NMJ (Koles et al., 2012; Korkut et al., 2013). We therefore examined whether expressing Rab11 dominant-negative (Rab11-DN) specifically in neurons induced a change in the levels of *darc1* RNA or protein in the postsynaptic region. We observed that this manipulation resulted in a highly significant reduction in *darc1* RNA and protein in the postsynaptic region (Fig. 2G,K,Q,R). Interestingly, when expressing Rab11DN in neurons, we observed a decrease in dArc1 levels in both the pre- and postsynaptic compartments, suggesting that Rab11 could be required both for the transport and release of dArc1. To distinguish between these possibilities, we calculated the proportion postsynaptic dArc1 levels relative to presynaptic levels (postsynaptic dArc1 levels/presynaptic dArc1 levels). We found that this ratio was significantly decreased upon expressing Rab11DN in neurons (Fig. 2S). Together, these data provide additional evidence for the trans-synaptic transfer of *darc1* mRNA and/or protein.

To further support the above conclusion, we expressed a dArc1 transgene in neurons, in a $darc1^{E8}/darc1^{esm113}$ mutant background. The transgene was composed of the *darc1* open reading frame, plus the untranslated regions (UTR). This resulted in the presence of dArc1, not only in presynaptic boutons, but also at the postsynaptic region (Fig. 3A). Interestingly, expressing a dArc1 transgene lacking the 3′UTR resulted in accumulation of the dArc1 signal in presynaptic terminals, but virtually no signal was observed at the postsynaptic region (Fig. 3B,I). Notably, the distribution of dArc1 lacking the 3′UTR was variable, being highly enriched at some synaptic boutons, and less enriched in others (Fig. 3C). The quantification of the dArc1 signal in Figure 3I omitted the highly-enriched boutons because in order for the quantification to be informative, the fluorescence levels must be in a linear, non-saturating range. Those boutons with very high expression were orders of magnitude brighter, such that the signal became saturated with confocal acquisition parameters that allowed us detect the postsynaptic signal. Notably, expressing the dArc1 construct including the 3′UTR in the muscles of the null mutant resulted in diffuse distribution of dArc1 signal throughout the muscle, and no postsynaptic enrichment was observed (Fig. 3D). Together, the above results provide compelling evidence that dArc1 protein and/or RNA are transferred from synaptic boutons to muscles, and that a normal dArc1 localization at postsynaptic sites depends on such transfer.

Yet, an alternative possibility is that alterations in *darc1* RNA and/or protein in presynaptic boutons might limit a signaling mechanism that induces *darc1* transcription or enrichment of *darc1* RNA and/or protein at the postsynaptic compartment. As RNA localization often depends on the RNA 3′UTR (Berkovits and Mayr, 2015), and as the lack of the *darc1* 3′UTR prevented the transfer of *darc1*, we determined if expressing *darc1 3′ UTR* alone in neurons was sufficient to allow the transfer. In these experiments *darc1-3′ UTR* was fused to GFP (Fig. 2U), expressed in neurons, and the levels of GFP signal at the postsynaptic compartment was assessed. As a control, we expressed GFP alone. Expressing *darc1-3′ UTR-GFP* (Fig. 3E), but not GFP alone (Fig. 3H,J), resulted in the presence of GFP signal in the muscle. Furthermore, expressing a shorter fragment of the 3′UTR (A-fragment [Fig. 2U]) fused to GFP in motorneurons was also sufficient for the transport of GFP (Fig.

3F,J). Interestingly, transfer of GFP was also observed when fusing it to a duplication of a *darc1* gene fragment (UGR [Fig. 2U]) that includes part of the 3′UTR (Fig. 3G,J; see below for further analysis of the UGR). Thus, *darc1* mRNA can be transferred from neurons to postsynaptic muscles in a manner dependent on its 3′UTR.

Notably, expressing *darc1-3′ UTR-GFP* in neurons in a *darc1* mutant background partly but significantly inhibited the transfer of GFP (Fig. 3K, L,M). The potential implication of this result is explored below.

dArc1 resembles a fragment of a retrotransposon, and a spliced form of *copia* RNA is also loaded into EVs

In addition to the presence of retroviral Gag-like sequences (Abrusan et al., 2013b; Campillos et al., 2006) (Fig. 7A), structural analyses have revealed that the Arc Gag region resembles the three-dimensional structure of the HIV virus Gag region (Zhang et al., 2015). Given that retroviruses are also similar to retrotransposons, which are present throughout the mammalian and fly genomes, we analyzed the S2 deep sequencing data using an algorithm designed to identify transposable elements, which are typically masked by the standard genome browsing algorithms. Strikingly, we found that *copia* mRNA, a common *Drosophila* retrotransposon, was highly enriched in S2 EVs (Fig. 4A). Closer examination of the sequence reads revealed that the *copia* RNA sequences present in EVs corresponded to a predicted spliced short *copia* (*copia*^{S}) species consisting primarily of the Gag region (Fig. 4B). This is in contrast to the cellular Copia, which has RNA-seq reads representing the whole transcript (Fig. S2). The *copia*^{S} isoform appeared to be selectively loaded into EVs as the ratio of *copia*^{S}/full length *copia* (*copia*^{L}) was 12.4/1 in the in the EV fraction, compared to 1.4/1 in the cell. To ascertain if Copia protein was also present in EVs we performed a mass spectrometry-based proteomic analysis of the S2 cell EV fraction. Notably, we found that the short Copia protein isoform was enriched in EVs (Fig. 4C).

dArc1 and dArc2 proteins are also present in EVs, and dArc1 protein binds mRNA

Given that both Copia^{S} protein and *copia*^{S} RNA were found in S2 EVs, we also determined if dArc1 protein, in addition to *darc1* mRNA, was similarly enriched in S2 EVs. To determine the relative abundance and enrichment of EV proteins compared to those in the cell, we performed mass spectrometry-based proteomic analysis of EVs compared to total cell proteins. Both dArc1 and dArc2 proteins were highly enriched in EVs compared to cellular proteins (Fig. 4C). Interestingly, our mRNA expression analysis did not reveal any enrichment of *darc2* mRNA in the EV fraction. The dArc2 ORF has 52.2% identity and 71.6% similarity with the dArc1 ORF, but lacks the putative C-terminal zinc finger domain, as well as the long *darc1* 3′UTR mRNA sequences present in *darc1*.

The Gag region of retroviruses binds to and packages retroviral gRNA. Thus, the enrichment of both dArc1 protein and mRNA in EVs and their similarity to Gag sequences raised the question as to whether dArc1 protein could bind its own mRNA *in vivo*. This was addressed by conducting RNA immunoprecipitation (RIP) experiments using S2 cell and larval body wall muscle extracts, gel shift assays, and *in vitro* binding assays. In the RIP experiments, anti-dArc1 was used to immunoprecipitate dArc1 protein and the immunoprecipitate was

analyzed by qRT-PCR to determine if *darc1* mRNA was present in this fraction. The dArc1 antibody co-immunoprecipitated *darc1* mRNA in both S2 cells and body wall muscle preparations (Fig. 4D,E). In contrast, no co-precipitation of other RNAs, such as *18s, eEf1a1,* and *copia* was observed (Fig. 4E), showing that the binding of dArc1 with its own mRNA has some degree of specificity *in vivo*. This is consistent with the idea that like retroviral Gag proteins, dArc1 exists in a complex with its own mRNA *in vivo*.

To further explore the binding of dArc1 to its own transcript *in vivo*, we expressed *darc1-3′ UTR-GFP* or *GFP* alone in larval neurons, immunoprecipitated dArc1 from extracts of body wall muscles derived from the above larvae, and tested the precipitate for the presence of *GFP* mRNA by qRT-PCR. Anti-dArc1 antibodies immunoprecipitated *GFP* RNA only when GFP was fused to the *darc1* 3′UTR, but not when GFP was expressed alone (Fig. 4F), in agreement with the model that dArc1 protein binds its own 3′UTR *in vivo*.

We next tested whether purified dArc1 is capable of directly binding RNA. We found, by co-incubating dArc1 with biotinylated control mRNA or biotinylated *darc1* mRNA, that dArc1 protein is immobilized on streptavidin-labelled beads (Fig. 4G). We next attempted electrophoretic mobility assays with both biotinylated or radiolabeled mRNAs but were unable to convincingly demonstrate specificity of dArc1 for its own mRNA versus controls. This is consistent with published observations showing that HIV-1 Gag proteins associate specifically with HIV gRNA *in vivo*, but that this binding specificity is lost *in vitro* (Comas-Garcia et al., 2016).

dArc1 protein assembles into capsid like structures

We noted that cleaving the HIS-MBP tag after affinity purification of bacterially produced dArc1 protein resulted in the formation of a precipitate. Given that dArc1 resembles a Gag protein, and that retroviral Gag proteins have the ability to auto-assemble into capsids, we examined the precipitate at the EM level by negative staining. Notably, we observed the presence of round structures of about 39.3±5.2 nm (Fig. 5A, B), which resembled HIV capsids. Thus, dArc1 appears to auto-assemble, and together with its ability to bind its own RNA *in vivo*, it is reasonable to suggest that has some properties similar to retroviruses.

Owing to the viral properties of dArc1 and we next sought to determine whether we could observe the dArc1 capsid-like structures in our EV preparations (Fig. S3A). In these experiments, the EV preparation was treated with saponin, to lyse EVs, and the resulting preparation examined by EM. Remarkably, we did observe the presence of ~40 nm round structures resembling the capsid-like elements obtained from purified dArc1 (Fig. 5C,D). Unlike those in purified protein, however, the capsid-like structures derived from EVs appeared electron dense, perhaps indicating the presence of RNA within them. To confirm if the ~40 nm structures observed in EVs contained dArc1 protein, we immunolabeled the grids with anti-dArc1 antibodies and 10nm gold conjugated secondary antibody. We found that many (Fig. 5E,F,G; black arrows;), but not all (Fig. 5E; white arrows) of the capsid-like structures contained gold granules (Fig. S3 for controls). This might be due to gold-free secondary, to the stringency of the washes during antibody staining, or to the presence of other capsid-like structures formed by alternative Gags.

dArc1 is involved in synaptic plasticity at the NMJ

We then examined the role of dArc1 during NMJ expansion, a process occurring throughout larval development, involving the addition of new synaptic boutons (Budnik et al., 1990). In addition, we tested its role in rapid activity-dependent synaptic bouton formation (Ataman et al., 2008). We found a drastic reduction in bouton numbers in 3rd instar (the last stage of larval development prior to metamorphosis) *darc1* null mutant larvae compared to controls (Fig. 6A,B,C,E,F,G,I). A similar result was observed upon expressing dArc1-RNAi in motorneurons (Fig. 6D,H,I). This suggests that a reduction of dArc1 in motorneurons inhibits synaptic expansion during larval development. Consistent with this model, presynaptic expression of a genomic *darc1* rescue construct in motorneurons completely rescued the reduced number of synaptic boutons resulting from eliminating or decreasing dArc1 levels (Fig. 6I). In contrast, expressing the *darc1* rescue construct in postsynaptic muscles, or eliminating its 3′UTR, did not rescue the mutant phenotype (Fig. 6I).

NMJ expansion involves the transient formation of immature synaptic boutons (ghost boutons) devoid of neurotransmitter release sites and postsynaptic proteins and specializations (Ataman et al., 2008; Koon et al., 2011). At the postsynaptic side, this is followed by the recruitment of postsynaptic proteins and formation of postsynaptic structures. Several mutations in genes required for NMJ development result in a reduced number of synaptic boutons and an accumulation of ghost boutons (Ataman et al., 2006; Harris et al., 2016). We found that, in addition to a reduction in bouton numbers, transallelic *darc1* mutations or *darc1* downregulation in neurons resulted in an accumulation of ghost boutons (Fig. 6F,G,H,J). As with the number of synaptic boutons, this phenotype was completely rescued by expressing the genomic *darc1* rescue construct in neurons, but not in muscles (Fig. 6J). Moreover, expressing a *darc1* transgene lacking the 3′UTR in neurons or muscles did not result in rescue.

NMJ expansion can be stimulated by increased synaptic activity during larval development (Ataman et al., 2008; Budnik et al., 1990). In addition, acute spaced stimulation of motorneurons gives rise to the rapid formation of ghost boutons, some of which subsequently undergo maturation (Ataman et al., 2008). To determine if dArc1 was required for this activity-dependent new bouton formation, we reduced dArc1 levels by expressing dArc1-RNAi in neurons. While the formation of ghost boutons upon spaced stimulation was normal in control animals, it was significantly reduced upon dArc1 downregulation (Fig. 6K,L,M,N,O). Thus, like mammalian Arc, *darc1* is required for both developmental and acute forms of synaptic plasticity.

The *darc1* genomic region is polymorphic and duplications of *darc1* sequences in this region downregulate *darc1* expression

It has been previously reported that, in contrast to our observations, dArc1 is not involved in synaptic plasticity (Mattaliano et al., 2007). To determine the potential reason for this discrepancy, we first sequenced the *darc1* genomic region of the wild type strain Canton-S (CS). Surprisingly, a neighboring gene annotated as pseudo-gene (referred to here as UGR) in the fly genome and located between *darc1* and *darc2* was absent in CS (Fig. 7A). The annotated *Drosophila* genome sequence was derived from a wild type strain different than

CS, Oregon-R (OR). Thus, there is a polymorphism in the *darc1-darc2* intergenic region locus between CS and OR wild type strain. Closer analysis of the UGR revealed that it was a duplication of a fragment of the *darc1* open reading frame (ORF) and part of its 3′UTR (Fig. 7A). To determine the potential impact of the UGR element in the OR strain, we compared *darc1* mRNA and protein levels in CS and OR. Notably, *darc1* RNA and protein levels were drastically reduced in OR compared to CS (Fig. 7B, Fig. S4). In addition, the number of synaptic boutons was significantly reduced in OR (Fig. 7C,D,E). We propose that the difference between our *darc1* mutant analysis and the previous report might arise from this difference between strains. Interestingly, upon sequencing the *darc1-darc2* intergenic region from S2 cells, which were generated from OR approximately 40 years ago (Schneider, 1972), we found that it lacks the UGR which raises the possibility that the UGR is a relatively recent divergence.

Discussion

Here we report a mechanism of trans-synaptic communication with several properties resembling retroviruses and retrotransposons, for the trans-synaptic transport of a Gag-related endogenous protein, dArc1, and its mRNA. dArc1 protein associates with the 3′UTR of its own transcript in vivo, and is transported, likely through EVs, from presynaptic boutons to the postsynaptic region of the Drosophila NMJ (Fig. 7F). This mechanism is required for proper synapse maturation during development and for activity-dependent synapse formation. We also provide evidence that, similarly, both Gag protein and RNA sequences from the retrotransposon Copia are loaded into EVs and released by cells, indicating either the domestication of viral mechanisms to shuttle material across cells, or the co-option of an endogenous cellular mechanism for viral infection.

Retroviruses and trans-synaptic transport of *darc1* RNA and protein

Multiple lines of evidence support the idea that dArc1 uses certain retroviral-like mechanisms to transfer a signal from the presynaptic compartment to the postsynaptic site required for NMJ expansion during development and for acute activity-dependent synaptic plasticity (Fig. 7F). (1) much like a viral capsid binds its own transcript, dArc1 protein interacts with the *darc1* mRNA, specifically its 3′UTR. It remains to be determined if dArc1 directly binds to its own transcript and if this binding is needed for EV loading of transcript and how dArc1 protein itself is loaded into EVs. (2) Like retroviruses, *darc1* RNA and protein are transmitted from cell to cell as determined by our observations of trans-synaptic transfer of wild type dArc1 protein and mRNA. (3) Arc protein appears to self-assemble forming capsid-like structures that are released from cells and can be extracted from exosome preparations. (4) The transfer appeared to be unidirectional, as postsynaptic muscle *darc1* mRNA and dArc1 protein levels were decreased when expressing dArc1-RNAi in neurons but not in muscles. The inability of dArc1-RNAi to downregulate *darc1* mRNA might be due to *darc1* RNA, at the postsynaptic region, being inaccessible to the RNAi machinery (e.g. D2 bodies (Nishida et al., 2013)). In our experiments dArc1-RNAi was expressed with the UAS/Gal4 system, which requires its transcription and export from the nucleus. In contrast, our experiments suggest that postsynaptic *darc1* mRNA and protein are locally derived from the presynaptic neuron, which likely determines their postsynaptic

localization. Indeed, expressing a dArc1 transgene in muscle did not result in synaptic localization of the transgenic protein. Another possible explanation of the resistance of postsynaptic Arc mRNA to postsynaptic RNAi is the ability of Arc protein to multimerize (Myrum et al., 2015) to form a capsid which protects *dArc1* RNA. Future studies will determine how *darc1* mRNA is unpackaged post-transfer from its Gag capsid to carry out its function and what processes are regulated by dArc1 leading to synapse growth and maturation.

Supporting the model that dArc1 takes advantage of viral properties for trans-synaptic signaling is our observation with a common endogenous fly retrotransposon, Copia. Retrotransposons like Copia contain the entire set of genes present in a retroviral genome except for envelope genes (Nefedova and Kim, 2017). Thus, unlike retroviruses, retrotransposons are thought not to be transferred between cells. Nevertheless, we found that both *copia* RNA and protein were released from cells via EVs which likely allows them to spread to neighboring cells. Strikingly, the Gag-encoding truncated region of *copia* RNA and protein were the predominant forms in S2 cell EVs. This short form does not encode the proteins necessary for Copia replication and integration into the genome, supporting the idea that this type of transcellular communication simply uses the RNA-binding properties of Gags to transport RNAs across cells.

The ORF of mammalian Arc and *darc1* are largely comprised of regions derived of viral-like Gag sequences, likely the remnants of an earlier transposon insertion, and previous work showed that the Gag region of Arc can fold like a viral capsid (Zhang et al., 2015). There are over 30 other proteins in Drosophila that have significant portions of their coding region comprised of Gag like sequences (Abrusan et al., 2013a). Both the fly and mammalian genomes contain a large proportion (~40%) of transposable elements (Lander et al., 2001), so far referred to as “junk DNA”. Our results raise the provocative idea that other Gag-related proteins and Gag-containing transposons might have a physiological function in cell-cell communications. This would explain the retention of retrotransposons through evolution. In addition, it is possible that the Gag-containing proteins encoded in the fly genome could represent the serendipitous integration of a retrotransposon into a functional gene, similarly to how dArc1 was likely created. Future studies geared to understanding the function of these Gag proteins as well as Gag-encoding transposons or transposon fragments will be needed to address these possibilities.

darc1-3′UTR as a mechanism of dArc1 loading into EVs

Drosophila Arc1 and Arc2 appear to result from a genomic duplication event and are solely composed of a Gypsy transposon-derived Gag domain. While the ORF of *darc1* and *darc2* are highly conserved, they differ vastly in their 3′UTR. Our studies with a GFP reporter show that the 3′UTR of *darc1* mRNA is necessary and sufficient for the transport and accumulation of *darc1* postsynaptically. This suggests that the 3′UTR of *darc1* imparts some function needed to load *darc1* mRNAs into EVs. In this regard, it’s interesting to note that the dArc2 protein, but not its mRNA, is enriched in EVs. While the protein and mRNA sequences of *darc1* and *darc2* are very similar, they differ dramatically in the 3′UTR, which in the case of *darc2* is much shorter. We hypothesize that this difference might explain the

absence of *darc2* mRNA in EVs. Our data suggests that *darc1* mRNA may prove to be a powerful model to understand EV RNA loading *in vivo*. Alternatively, as reported in the companion paper (Day et al.), RNA binding to Gag proteins might be required to assemble a capsid, with might be needed for EV loading. The rat *Arc 3′ UTR* contains Gypsy-like sequences, transposon sequences similar to those of *darc1*. Since these genes most likely evolved independently (Abrusan et al., 2013b) (also see the companion paper; Day et al.) the similarity of the mammalian and fly Arc proteins and mRNAs indicates the possibility of convergent evolution of this mechanism of trans-cellular communication.

Trans-synaptic dArc1 transfer in *Drosophila* synapse development and plasticity

Our studies of *darc1* mutants, dArc1-RNAi, and expression of transgenic dArc1 variants suggest that the transfer of dArc1 is required for normal expansion of the NMJ, synaptic bouton maturation, and activity-dependent synaptic bouton formation. For example, expressing a dArc1 transgene lacking the 3′UTR in neurons, while resulting in the localization of the transgenic protein at presynaptic boutons, it is not transferred to the postsynaptic region and fails to rescue mutant phenotypes at the NMJ. In contrast, expressing a transfer-competent dArc1 transgene, containing the 3′UTR, results in complete rescue. Therefore, it is not just the presence of dArc1 in presynaptic terminals, but the actual transfer to the postsynaptic region which is required for dArc1 function at the NMJ. This is also supported by our finding that expressing dArc1 containing the 3′UTR in muscles alone did not result in normal postsynaptic dArc1 localization, nor did it rescue mutant phenotypes at the NMJ. Thus, both normal postsynaptic localization of dArc1 and its function in synaptic development and plasticity requires dArc1 transfer from the presynaptic terminus. The requirement of d*arc1*-3′UTR also provides support to the idea that *darc1* mRNA, and not just dArc protein is transferred, which is also supported by our finding of both dArc1 protein and RNA in EVs.

Previous studies show that the transfer or release of EV proteins, such as Evi and Wg, is enhanced by electrical activity (Ataman et al., 2006), and similar observations have been made with cultured mammalian neurons and glia (Faure et al., 2006; Fruhbeis et al., 2013). This opens the possibility that dArc1 might be delivered to postsynaptic sites in an activity-dependent fashion. This would allow the functional modification of specific postsynaptic sites.

Trans-synaptic transfer as a general mechanism of Arc/dArc1 function

In mammals Arc is a master regulator of synaptic plasticity, being involved in many aspects of synapse formation, maturation and plasticity, as well as in learning and memory (Shepherd and Bear, 2011). Arc expression is induced by synaptic activity and its mRNA becomes localized to active dendritic spines, where it contributes to local translation during synaptic plasticity (Farris et al., 2014). Not surprisingly, in humans, mutations in Arc are associated with multiple neurological disorders affecting synapses, including autism spectrum disorders (Alhowikan, 2016), Angelman syndrome (Cao et al., 2013), and schizophrenia (Fromer et al., 2014). While some mechanisms of Arc function, such as its involvement in trafficking of glutamate receptors during plasticity (Chowdhury et al., 2006) are beginning to be elucidated, the extent of its roles remain to be deciphered. In this and the

companion paper (Day et al.), we reveal a highly significant Arc/dArc1 role in trans-synaptic signaling. The studies reveal the significance of a long-noted but mysterious feature of Arc/dArc1 protein, its resemblance to retroviral Gags. Together with the companion paper we show that, like retroviruses, Arc/dArc1 proteins can form capsids capable of packaging RNAs. These capsids are loaded into EV-like vesicles that can be released from synaptic sites and taken up by synaptic partners. While a functional role in synaptic development and plasticity is documented here at the *Drosophila* NMJ, the significance of this transfer at mammalian synapses remains to be determined. In Drosophila dArc1 protein and mRNA are present both inside presynaptic boutons and at the postsynaptic muscle region (this report). In contrast, Arc has been reported to localize exclusively in dendrites, and not at presynaptic sites (Lyford et al., 1995). The finding that mammalian Arc is also released in EVs (Day et al) raises the possibility that this release might serve as a signaling mechanism between dendritic spines. However, if this signaling process plays a role in synaptic plasticity, it would call into question the synapse-specificity of synaptic plasticity documented in the mammalian brain (Viola et al., 2014). An alternative possibility is that mammalian Arc, while primarily being localized at postsynaptic sites, it is also present in lesser amounts at presynaptic terminals. Indeed, in the fly, most of the dArc1 protein and RNA is present at the postsynaptic region. Studies of Arc downregulation in presynaptic neurons and its effect in the localization of Arc at dendritic spines, may serve to distinguish between these possibilities.

STAR Methods

Further information and requests for resources and reagents should be directed to and will be fulfilled by the Lead Contact, Vivian Budnik (Vivian.Budnik@umassmed.edu).

Experimental Model and Subject Details

The following fly lines were used, UAS-dArc1-RNAi1 (31122, Vienna *Drosophila* Research Center), UAS-Rab11DN[N124I] (Satoh et al., 2005). UAS-dArc1-RNAi2 (see below), the wild type strain, CantonS (CS) (1, Bloomington *Drosophila* stock center, BDSC), the wild type strain, OregonR (OR) (6362, BDSC), UAS-GFP (5431, BDSC), UAS-*darc1*-3′UTR-GFP (see below), UAS-darc1-A-fragment-GFP (see below), UAS-darc1-UGR-GFP (see below), C380-Gal4 and C57-Gal4 (Budnik, 1996). Unless otherwise mentioned in the text, for constiency, female 3rd Instar larvae were dissected for NMJ preparations.

Method Details

Fly husbandry—All flies were raised on standard molasses formulation food at either 25°C (most crosses) or 29°C (RNAi crosses).

Generation of a dArc1null allele—A mutant allele of *darc1* was generated by Crispr/Cas9-mediated genomic engineering as previously described (Port and Bullock, 2016). Briefly, sequences encoding two single-guide RNAs (sgRNA1 and sgRNA2) targeting *darc1* gene flanking sites which were predicted to have no off-targets (flyCRISPR target finder; (http://tools.flycrispr.molbio.wisc.edu/targetFinder/) (Gratz et al., 2014) were cloned into the pCFD4 plasmid. This construct was injected into Actin-Cas9 expressing embryos and flies

containing potentially mutant chromosomes were captured over a balancer chromosome and made into stocks. The stocks were subsequently screened for the desired deletion by PCR, employing deletion-flanking primers sets. Sequencing of PCR products generated from the *darc1*^{E8} line revealed the expected deletion.

Constructs: The sequence of constructs made for this paper can be found in Table S1 DNA sequences of constructs used. Related to STAR Methods.

The UAS-darc1-3′UTR-GFP constructs were cloned into pAWG vector using the Gateway system (ThermoFisher). The GFP with resulting 3′UTR fragments were amplified out of this construct, and cloned into pENTR/DTOPO. The resulting construct was finally cloned into the pTWM construct, containing an attB site for targeted genomic insertion. The *darc1* sequences are in Table S1.

The UAS-dArc1-RNAi2 construct was cloned by first amplifying a dArc1 fragment, that was non-overlapping with the VDRC 31122 line, using RNAi2 forward and reverse primers.

The PCR product was cloned into PENTR-DTOPO (ThermoFisher), and then, using the Gateway system (ThermoFisher), it was cloned into pWalium10. All constructs were then injected into flies and integrated at site attP2 on the third chromosome, through targeted integration by BestGene.

The UAS-dArc1 rescue transgene was synthesized (Genscript) and using the Gateway system (ThermoFisher), cloned into the pTWM vector. The sequence of the *darc1* rescue construct is included in Table S1.

Immunocytochemistry and antibodies: Body wall muscles from third instar larva were dissected in low calcium (0.1mM Calcium) HL3 saline (Stewart et al., 1994) and fixed in either Bouin's fixative (0.9% picric acid, 5% acetic acid, 9% formaldehyde, 2.5–5% methanol) or 4% paraformaldehyde in 0.1 M phosphate buffer. Fixed larvae were washed and permeabilized in PBT (0.1 M phosphate buffer; 0.2% (v/v) Triton X-100) and incubated in primary antibody overnight at 4°C. Samples were washed three times with PBT and incubated in secondary antibodies for 2 hours at room temperature. After incubation with secondary antibodies, samples were washed thrice with PBT and mounted in Vectashield (Vector Laboratories). The following antibodies were used: anti-dArc1 (see below 1:500 for immunocytochemistry (ICC), 1:1000 for Western blots), anti-GFP (Developmental Studies Hybridoma Bank (DSHB), 4C9, 1:200), and rabbit anti-DLG, 1:40,000 (Koh et al., 1999). DyLight-conjugated secondary antibodies were from Jackson ImmunoResearch (DyLight-594-conjugated goat anti-HRP, DyLight-488-conjugated anti-mouse or anti-rabbit or, DyLight-594-conjugated anti-mouse or anti-rabbit) and were used at 1:200 dilution.

dArc1 antibodies were generated against the first 56 amino acids of dArc1 by immunizing rabbits and rats with purified 6X His tagged peptides (Pocono Rabbit Farm and Laboratory). A synthetic gene representing the first 56 amino acids was synthesized into pET151 (ThermoFisher), transfected into BL21(DE3) bacterial cells (ThermoFisher) and His tagged dArc1 peptide was purified on a nickel column (Pierce).

Fluorescent in situ hybridization (FISH): In situ hybridization was performed as described previously (Speese et al., 2012) with minor modifications. Briefly larval body wall muscles were dissected as described above and fixed with 4% paraformaldyhyde for 30min. Preparations were then washed three times, 10 min each, with 0.2%PBT with RNasin (Promega). Samples were equilibrated with hybridization buffer (2XSSC, 10% dextran sulfate, RNasin (Promega), 50% formamide). Gene specific probes (125ng probe, 1.25μg salmon sperm DNA, 1.25μg yeast tRNA) were heated to 80°C for 5min and chilled on ice immediately. Probes were then combined with equal volumes of 2X hybridization buffer (final concentration of 2.5ng/μL gene specific probes). Samples were incubated with probes for 3 hours at 37°C. From this point onward, the protocol was the same as in Speese et al 2012 (Speese et al., 2012). To visualize synaptic boutons, samples were colabeled with goat anti-HRP-Dylight594 (Jackson ImmunoResearch).

Probe preparation: Probe preparation was the same as described previously(Speese et al., 2012). Briefly, probes were designed based on the cDNA sequences of dArc1 and amplified using dArc1 probe primers. The probes were produced by nick translation of the PCR product (Bionick; ThermoFisher) with digoxigenin-11-dUTP (Roche) for 2.5hrs at 18°C, and the reaction was inactivated by heating to 65°C for 10min. Probes were precipitated and resuspended in formamide and stored at −80°C. Blocking probe against shibire was prepared using the same method except dTTP was used instead of digoxigenin-labeled dUTP.

Confocal Microscopy and Signal Intensity Measurements: Images shown in figures were acquired on Zeiss LSM 700 or LSM 800 confocal microscope equipped with a Zeiss 63X Plan-Apochromat 1.4 NA DIC oil immersion objective. For quantification of signal intensity using Volocity Software (version 6.3.1), NMJs were imaged at identical settings for control and experimental groups processed simultaneously on a Zeiss Axioplan microscope equipped with a Yokogawa CSU10 spinning disk confocal scanning unit and a Hamamatsu 9100 EM-CCD camera (512 × 512) and a 40X EC-Plan-NeoFluar 1.3 NA objective. Briefly, after image acquisition, the bouton volume bounded by HRP staining was selected using Volocity, and fluorescence intensity inside was measured. To calculate the postsynaptic area, the presynaptic bouton selection was dilated by 8 iterations, the HRP containing volume was subtracted and the intensity within the remaining volume was measured. Intensity was determined as the sum of total pixel intensity in each volume (pre- and postsynaptic) and normalized to bouton volume, as described previously (Ramachandran et al., 2009).

Exosome Preparation: Exosomes were prepared from S2 cells that were cultured in serum-free medium to avoid contamination from Bovine serum exosomes. Cultures were grown in spinner flasks (BellCo Glass Inc.) at 22 °C and harvested at 1–1.5 × 10^6 cells/mL density. Exosomes were further purified as described previously (Koles et al., 2012) but detailed as follows. The cells from 500 ml of culture were pelleted at 300 × *g* for 5 min, the supernatant was then spun for10 min at 2000 × *g*, to clear dead cells. To remove large cellular debris the samplers were then centrifuged at 10,000 × *g* for 30 min to remove. To collect exosomes the samples were spun at 100,000 × *g* for 70 min, the pellet was resuspended in PBS. Tris/sucrose/D_2O (200 mM, 30% (w/v), 50% (v/v)) was mixed together and put into a centrifuge tube to form a sucrose cushion on top of which the exosome pellet was layered, then

centrifuged in an SW28 ultracentrifuge rotor at 100,000 × *g* for 75 min. Using a syringe through the side of the tube 3.5ml of the Tris/sucrose/PBS interface was collected. To remove the sucrose and D_2O 60 ml of PBS was added to samples which were then centrifuged at100,000 × *g* for 70 min. The final pellet representing the purified exosomes were resuspended in 500ul of PBS and either processed for future experiments or stored at −80 °C.

RNA sequencing: Exosomes were treated with micrococcal nuclease (NEB) for 1 hour at 37°C, and then both exosomes and cell pellets we re treated with RLT buffer (Qiagen) and RNA was extracted using RNeasy micro Kit (Qiagen). Libraries were prepared using NEBNext Ultra directional RNA library prep kit for Illumina sequencing. Library 1 was subjected to single end sequencing with 18934428 and 13513146 reads for cell and exosomes respectively. Libraries 2, 3 and 4 were pair end-sequenced using miSeq illumina. While library 2 had 1745707 exosome and 2188190 cell reads, library 3 had 2921143 exosome and 1823805 cell reads and library 4 had 3649518 exosome and 5047915 cell reads. Reads from each library were sorted by barcode, and adapter sequences removed. Reads were then mapped using TopHat2 (Kim et al., 2013) to the *Drosophila* genome. Transcript expression was measured using Cufflinks (Trapnell et al., 2012), and differential expression was determined using DeSeq2 (Love et al., 2014). For transposon mapping reads, reads from each library were mapped to common *Drosophila* transposon sequences using Bowtie2 (Langmead et al., 2009). Expression was then measured using eXpress (Roberts and Pachter, 2013) and DeSeq2.

Biotinylated RNA pull down assay: Reagents used for this assay were from the LightShift™ Chemiluminescent RNA EMSA Kit (ThermoFisher, Catalog number: 20158). For dArc1 protein, the dArc1 ORF was cloned into the pDEST-His-MBP(Nallamsetty et al., 2005) vector using the Gateway system (ThermoFisher). Protein was then expressed in Bl21(DE3) *E. coli* (ThermoFisher) and purified by nickel-chelation chromatography (New England Biolabs). The 3′UTR of *darc1* was cloned into pDEST17 (ThermoFisher) using the Gateway system (ThermoFisher). The resulting vector was then digested with EcoRV, and then incubated overnight with T7 RNA polymerase (ThermoFisher). The subsequent RNA was then purified through lithium chloride precipitation, and then end labeled using 3′ Biotinylation (ThermoFisher). For competition assays, the specific competitor was the unlabeled 3′UTR transcript, while the unspecific competitor was generated from an empty pDEST17 vector linearized with SmaI, incubated overnight with T7 RNA polymerase, and purified through lithium chloride precipitation as above. Each binding assay was carried out using 80ng of labelled *darc1* 3′UTR and 9μg of dArc1 protein. After incubating for 30 minutes, 25μl of washed Steptavidin magnetic beads (ThermoFisher) was added. The beads were washed 3X with binding buffer, then protein loading buffer was added, the samples were boiled, run on a stain-free 4–20% acrylamide gel (Bio-Rad), and imaged in a ChemiDoc Imaging System (BioRad).

Sample preparation for LC/MS/MS: Purified exosomes and cell pellets were diluted in loading buffer (see below), incubated at 95°C for 1 5 min, and resolved by SDS-PAGE in a

4–20% gradient gel under reducing and denaturing conditions. Proteins were run 2cm into the resolving gel, excised, and processed for mass spec analysis.

LC/MS/MS: Gel slices were cut into 1×1 mm pieces and placed in 1.5ml Eppendorf tubes with 1ml of water for 30 min. The water was removed and 150μL of 250mM ammonium bicarbonate was added. For reduction, 20μL of a 45mM solution of 1,4 dithiothreitol (DTT) was added and the samples were incubated at 50°C for 30 min. The samples were cooled to room temperature and then, for alkylation, 20μL of a 100mM iodoacetamide solution was added and allowed to react for 30 min. The gel slices were washed 2 X with 1ml water aliquots. The water was removed, 1ml of 50:50 (50mM ammonium: bicarbonate: acetonitrile) was added to each tube, and samples were incubated at room temperature for 1hr. The solution was then removed and 200μL of acetonitrile was added to each tube at which point the gels slices turned opaque white. The acetonitrile was removed and gel slices were further dried in a Speed Vac. Gel slices were rehydrated in 100μL of 4ng/μL trypsin (Sigma or Promega sequencing grade) in 0.01% ProteaseMAX Surfactant (Promega): 50mM ammonium bicarbonate. Additional bicarbonate buffer was added to ensure complete submersion of the gel slices. Samples were incubated at 37°C for 21hrs. The supernatant of each sample was then removed and placed in a separate 1.5mL eppendorf tube. Gel slices were further dehydrated with 100μL of 80:20 (acetonitrile: 1% formic acid). The extract was combined with the supernatants of each sample. The samples were then dried down in a Speed Vac. Samples were dissolved in 25μL of 5% acetonitrile in 0.1% trifluroacetic acid prior to injection on LC/MS/MS. A 3.0μl aliquot was directly injected onto a custom packed 2cm × 100μm C18 Magic 5μ particle trap column. Peptides were then eluted and sprayed from a custom packed emitter (75μm × 25cm C18 Magic 3μm particle) with a linear gradient from 95% solvent A (0.1% formic acid in water) to 35% solvent B (0.1% formic acid in acetonitrile) in 90 minutes at a flow rate of 300 nl/min on a Waters Nano Acquity UPLC system. Data-dependent acquisitions were performed on a Q Exactive mass spectrometer (Thermo Scientific) according to an experiment where full MS scans from 300–1750 m/z were acquired at a resolution of 70,000 followed by 10 MS/MS scans acquired under HCD fragmentation at a resolution of 17,500 with an isolation width of 1.6 Da. Raw data files were processed with Proteome Discoverer (version 1.4) prior to searching with Mascot Server (version 2.5) against the Uniprot database. Search parameters utilized were fully tryptic with 2 missed cleavages, parent mass tolerances of 10 ppm and fragment mass tolerances of 0.05 Da. A fixed modification of carbamidomethyl cysteine and variable modifications of acetyl (protein N-term), pyro glutamic for N-term glutamine, oxidation of methionine and serine/threonine phosphorylation were considered. Search results were loaded into the Scaffold Viewer (Proteome Software, Inc.) for assessment of protein identification probabilities and label free quantitation.

RNA IP with Real time quantitative PCR: For S2 cell preparations, cells were raised in serum free medium, as above, and then centrifuged at 300 × g to pellet the cells. Once pelleted, cells were resuspended in RIPA buffer (Abcam), and homogenized using 0.5mm glass beads at 4°C using a BBX24B Bullet Blen der Blue homogenizer (Next Advance Inc.). Larval body wall muscles from wild type animals were homogenized in RIPA buffer (Abcam), and homogenized as above. Supernatants were cleared against magnetic beads

(Pierce), and then incubated with either anti-dArc1, or equal amounts of preimmune serum. Samples were incubated overnight with serum and magnetic beads, and washed several times with RIPA buffer. Finally, beads were either incubated directly with 5X loading buffer (4% SDS, 250mM Tris, Bromphenol blue, 30% glycerol, and 2-Mercaptoethanol) for Western blot, or RNA was eluted from the beads with RLT buffer (Qiagen) and then purified using the RNeasy micro kit (Qiagen). RNA samples from both conditions were DNase treated with TurboDNase (ThermoFisher) and then equal volumes were reverse transcribed into cDNA using Superscript III (ThermoFisher). The RT-quantitative PCRs were performed in triplicate in a 96-well plate (BioRad) using a CFX96 system (BioRad). For the reactions, a Sybr green master mix (ThermoFisher) was used with the gene specific primer sets for dArc1, Copia, GFP, dArc2 and 18S rRNA. RpL32 was used as a reference gene. All transcript levels were normalized to RpL32 transcript level, using the same cDNA template. Data were expressed in graphs as ΔC_T. For RTq-PCR on body wall preparations, 5 larvae per genotype were dissected and RNA was purified from Brains and body wall muscles separately using RNeasy kit (Qiagen). All cDNA for body wall preparation analysis was synthesized with 100ng of RNA, and then samples were treated as above for qRT-PCR.

Western Blotting: Extracts from RIP experiments were incubated at 95 °C for 15 min, and resolved by SDS-PAGE in a 4–20% gradient gel under reducing and denaturing conditions. Proteins were transferred onto nitrocellulose membrane (Bio-Rad) and blocked in 5% instant nonfat dry milk in TBST (50 mM Tris (pH 7.4), 150 mM NaCl, 0.05% Tween 20) and incubated with primary antibodies (diluted to working concentration in blocking solution) overnight at 4 °C. After washing in TBST, blots were incubated with HRP-conjugated secondary antibodies diluted to 1:3000 in blocking solution for 1 h at room temperature. Western blots were visualized using the SuperSignal West Femto Maximum Sensitivity Substrate kit (ThermoFisher). Blots were imaged using Chemidoc Touch imaging system (BioRad).

Activity Paradigm: Potassium stimulations were performed as in (Ataman et al., 2008). Briefly, larva were dissected in low calcium HL3 (Stewart et al., 1994) saline, and then pulsed with high potassium saline for 2 minutes, 3 times, each separated by 15 minutes of rest in normal saline. The final two stimulations were done for 4 and 6 minutes separated by 15 minutes of rest. Samples were then fixed and processed for immunocytochemistry.

dArc1 Capsid Formation: The *darc1* open reading frame was cloned into pENTR (Thermo Fisher), its sequence confirmed, and pENTR-Arc was subsequently recombined using LR Clonase (Thermo Fisher) with the pDEST-HisMbp Destination vector (Nallamsetty et al., 2005) to generate His-MBP-dArc1. Expression induction and purification under native conditions in a Ni-NTA column (Qiagen) were performed following standard procedures. To generate soluble protein for ultrastructural studies, protein was diluted to ~ 1 mg/ml and cleaved at 30 degrees C with AcTEV (Thermo-Fisher), followed by removal of the His-MBP tag and the His tagged TEV by binding to a Ni-NTA column and dialysis against PBS.

Electron Microscopy of dArc1 capsid: After formation of dArc1 capsids, the capsids were examined using negative staining. Capsids were fixed in 2% paraformaldehyde overnight at

4°C. 5μL of fixed capsids were spotted onto formvar coated grids. After 20 min absorption, grids were rinsed with PBS and then fixed with 1% glutaraldehyde for 5 min. Finally, samples were washed with water and then counter-stained with 2% w/v uranyl acetate, and blotted dry. Samples were imaged on an FEI EM 10 electron microscope at 80 kv.

ImmunoEM of Exosomes: Exosome preparations were fixed overnight in a final concentration of 2% paraformaldehyde (EM grade) at 4°C. After fixation, solution was gently pipetted up and down several times to resuspend exosomes. Formvar coated grids (EMS) were glow discharged, spotted with 4μl of exosomes, and incubated for 10 min at room temperature. Excess solution was removed by gently wicking liquid off of the grid on #50 filter paper. Grids were washed 2 times, 3 min each, in 100mM Tris, followed by 4 washes, 3 min each, in 100mM Tris + 50mM Glycine. Grids were blocked for 10 min with 100mM Tris + 0.1% BSA. After block, exosomes were either incubated in 100mM Tris (control) or lysed with 0.05% saponin in 100mM Tris. Grids were washed for 2 min with 100mM Tris followed by an anti-dArc1 antibody (1:500 in 100mM Tris) incubation for 1hr. Grids were then washed 5 times, 3 min each, in 100mM Tris, followed by a 30 min incubation with goat anti-rabbit conjugated to 10nm gold (Electron Microscopy Sciences) secondary (1:60 dilution in 100mM Tris). Grids were washed 8 times, 2 min each, in 100mM Tris, and then fixed with 1% glutaraldehyde in 100mM Tris for 1 min at room temperature. Finally, grids were washed again 8 times, 2 min each, with distilled water, and then negative stained with 1% uranyl acetate for 30 seconds. Grids were imaged on an FEI EM 10 as above.

Quantification and Statistical Analysis

Statistical analysis was performed using a Student's *t* test when a single experimental sample was compared with control. For comparison of multiple experimental groups, a one-way analysis of variance (ANOVA) was used followed by a Tukey's post hoc test. *, $p < 0.05$; **, $p < 0.001$; ***, $p < 0.0001$. Excel (Microsoft) and Kaleidograph (Synergy Software) were used to measure, standard deviations, standard errors and averages, as well as create graphs. Each figure contains relevant information as to the number of experimental repeats and other data needed to assess the accuracy of the data.

Data and Software Availability

Data Resources—The accession number for the raw and analyzed RNA-sequencing data reported in this paper is GEO:GSE104972

The mass spectrometry proteomics data have been deposited to the ProteomeXchange Consortium (Deutsch et al., 2017) via the PRIDE (Vizcaino et al., 2016) partner repository with the dataset identifier PXD008136 and 10.6019/PXD008136.

Supplementary Material

Refer to Web version on PubMed Central for supplementary material.

Acknowledgments

We thank the Bloomington *Drosophila* Stock Center and flybase (NIH P40OD018537) for providing stocks and managing the fly database, and the Vienna *Drosophila* Resource Center (VDRC). We thank Drs. Melissa Moore for valuable discussions and methodological guidance, Emiliano Riccio for help in library preparation in the initial stages of this project, and Franz Wendler for exosome preparation. We also thank Dr. Jason Shepherd for helpful discussions. This work was supported by NIH Grant R37MH070000 to VB.

References

Abrusan G, Szilagyi A, Zhang Y, Papp B. Turning gold into 'junk': transposable elements utilize central proteins of cellular networks. Nucleic Acids Res. 2013a; 41:3190–3200. doi:3110.1093/nar/gkt3011. Epub 2013 Jan 3121. [PubMed: 23341038]

Abrusan G, Szilagyi A, Zhang Y, Papp B. Turning gold into 'junk': transposable elements utilize central proteins of cellular networks. Nucleic Acids Res. 2013b; 41:3190–3200. [PubMed: 23341038]

Alenquer M, Amorim MJ. Exosome Biogenesis, Regulation, and Function in Viral Infection. Viruses. 2015; 7:5066–5083. doi:5010.3390/v7092862. [PubMed: 26393640]

Alhowikan AM. Activity-Regulated Cytoskeleton-Associated Protein Dysfunction May Contribute to Memory Disorder and Earlier Detection of Autism Spectrum Disorders. Med Princ Pract. 2016; 25:350–354. doi:310.1159/000445351. Epub 000442016 Mar 000445311. [PubMed: 26967659]

Ataman B, Ashley J, Gorczyca D, Gorczyca M, Mathew D, Wichmann C, Sigrist SJ, Budnik V. Nuclear trafficking of Drosophila Frizzled-2 during synapse development requires the PDZ protein dGRIP. Proc Natl Acad Sci U S A. 2006; 103:7841–7846. [PubMed: 16682643]

Ataman B, Ashley J, Gorczyca M, Ramachandran P, Fouquet W, Sigrist SJ, Budnik V. Rapid activity-dependent modifications in synaptic structure and function require bidirectional Wnt signaling. Neuron. 2008; 57:705–718. [PubMed: 18341991]

Basso M, Bonetto V. Extracellular Vesicles and a Novel Form of Communication in the Brain. Front Neurosci. 2016; 10:127. eCollection 02016. doi: 10.3389/fnins.2016.00127 [PubMed: 27065789]

Berkovits BD, Mayr C. Alternative 3′ UTRs act as scaffolds to regulate membrane protein localization. Nature. 2015; 522:363–367. doi:310.1038/nature14321. Epub 12015 Apr 14320. [PubMed: 25896326]

Budnik V. Synapse maturation and structural plasticity at Drosophila neuromuscular junctions. Curr Opin Neurobiol. 1996; 6:858–867. [PubMed: 9000022]

Budnik V, Koh YH, Guan B, Hartmann B, Hough C, Woods D, Gorczyca M. Regulation of synapse structure and function by the Drosophila tumor suppressor gene dlg. Neuron. 1996; 17:627–640. [PubMed: 8893021]

Budnik V, Zhong Y, Wu CF. Morphological plasticity of motor axons in Drosophila mutants with altered excitability. J Neurosci. 1990; 10:3754–3768. [PubMed: 1700086]

Campillos M, Doerks T, Shah PK, Bork P. Computational characterization of multiple Gag-like human proteins. Trends Genet. 2006; 22:585–589. Epub 2006 Sep 2018. [PubMed: 16979784]

Cao C, Rioult-Pedotti MS, Migani P, Yu CJ, Tiwari R, Parang K, Spaller MR, Goebel DJ, Marshall J. Impairment of TrkB-PSD-95 signaling in Angelman syndrome. PLoS Biol. 2013; 11:e1001478. [PubMed: 23424281]

Chen B. HIV Capsid Assembly, Mechanism, and Structure. Biochemistry. 2016; 55:2539–2552. doi: 2510.1021/acs.biochem.2536b00159. Epub 02016 Apr 00126. [PubMed: 27074418]

Chowdhury S, Shepherd JD, Okuno H, Lyford G, Petralia RS, Plath N, Kuhl D, Huganir RL, Worley PF. Arc/Arg3.1 interacts with the endocytic machinery to regulate AMPA receptor trafficking. Neuron. 2006; 52:445–459. [PubMed: 17088211]

Comas-Garcia M, Davis SR, Rein A. On the Selective Packaging of Genomic RNA by HIV-1. Viruses. 2016; 8

Deutsch EW, Csordas A, Sun Z, Jarnuczak A, Perez-Riverol Y, Ternent T, Campbell DS, Bernal-Llinares M, Okuda S, Kawano S, et al. The ProteomeXchange consortium in 2017: supporting the

cultural change in proteomics public data deposition. Nucleic Acids Res. 2017; 45:D1100–D1106. [PubMed: 27924013]

Dynes JL, Steward O. Dynamics of bidirectional transport of Arc mRNA in neuronal dendrites. J Comp Neurol. 2007; 500:433–447. [PubMed: 17120280]

Farris S, Lewandowski G, Cox CD, Steward O. Selective localization of arc mRNA in dendrites involves activity- and translation-dependent mRNA degradation. J Neurosci. 2014; 34:4481–4493. doi:4410.1523/JNEUROSCI.4944-4413.2014. [PubMed: 24671994]

Faure J, Lachenal G, Court M, Hirrlinger J, Chatellard-Causse C, Blot B, Grange J, Schoehn G, Goldberg Y, Boyer V, et al. Exosomes are released by cultured cortical neurones. Molecular and cellular neurosciences. 2006; 31:642–648. [PubMed: 16446100]

Fromer M, Pocklington AJ, Kavanagh DH, Williams HJ, Dwyer S, Gormley P, Georgieva L, Rees E, Palta P, Ruderfer DM, et al. De novo mutations in schizophrenia implicate synaptic networks. Nature. 2014; 506:179–184. doi:110.1038/nature12929. Epub 12014 Jan 12922. [PubMed: 24463507]

Fruhbeis C, Frohlich D, Kuo WP, Amphornrat J, Thilemann S, Saab AS, Kirchhoff F, Mobius W, Goebbels S, Nave KA, et al. Neurotransmitter-triggered transfer of exosomes mediates oligodendrocyte-neuron communication. PLoS Biol. 2013; 11:e1001604. doi:1001610.1001371/journal.pbio.1001604. Epub 1002013 Jul 1001609. [PubMed: 23874151]

Gratz SJ, Ukken FP, Rubinstein CD, Thiede G, Donohue LK, Cummings AM, O'Connor-Giles KM. Highly specific and efficient CRISPR/Cas9-catalyzed homology-directed repair in Drosophila. Genetics. 2014; 196:961–971. [PubMed: 24478335]

Harris KP, Akbergenova Y, Cho RW, Baas-Thomas MS, Littleton JT. Shank Modulates Postsynaptic Wnt Signaling to Regulate Synaptic Development. J Neurosci. 2016; 36:5820–5832. doi:5810.1523/JNEUROSCI.4279-5815.2016. [PubMed: 27225771]

Jan LY, Jan YN. Antibodies to horseradish peroxidase as specific neuronal markers in Drosophila and in grasshopper embryos. Proc Natl Acad Sci U S A. 1982; 79:2700–2704. [PubMed: 6806816]

Kim D, Pertea G, Trapnell C, Pimentel H, Kelley R, Salzberg SL. TopHat2: accurate alignment of transcriptomes in the presence of insertions, deletions and gene fusions. Genome Biol. 2013; 14:R36. [PubMed: 23618408]

Koh YH, Popova E, Thomas U, Griffith LC, Budnik V. Regulation of DLG localization at synapses by CaMKII-dependent phosphorylation. Cell. 1999; 98:353–363. [PubMed: 10458610]

Koles K, Nunnari J, Korkut C, Barria R, Brewer C, Li Y, Leszyk J, Zhang B, Budnik V. Mechanism of evenness interrupted (Evi)-exosome release at synaptic boutons. J Biol Chem. 2012; 287:16820–16834. [PubMed: 22437826]

Koon AC, Ashley J, Barria R, DasGupta S, Brain R, Waddell S, Alkema MJ, Budnik V. Autoregulatory and paracrine control of synaptic and behavioral plasticity by octopaminergic signaling. Nat Neurosci. 2011; 14:190–199. [PubMed: 21186359]

Korkut C, Ataman B, Ramachandran P, Ashley J, Barria R, Gherbesi N, Budnik V. Trans-synaptic transmission of vesicular Wnt signals through Evi/Wntless. Cell. 2009; 139:393–404. [PubMed: 19837038]

Korkut C, Li Y, Koles K, Brewer C, Ashley J, Yoshihara M, Budnik V. Regulation of postsynaptic retrograde signaling by presynaptic exosome release. Neuron. 2013; 77:1039–1039. [PubMed: 23522040]

Lander ES, Linton LM, Birren B, Nusbaum C, Zody MC, Baldwin J, Devon K, Dewar K, Doyle M, FitzHugh W, et al. Initial sequencing and analysis of the human genome. Nature. 2001; 409:860–921. [PubMed: 11237011]

Langmead B, Trapnell C, Pop M, Salzberg SL. Ultrafast and memory-efficient alignment of short DNA sequences to the human genome. Genome Biol. 2009; 10:R25. [PubMed: 19261174]

Lefebvre FA, Benoit Bouvrette LP, Perras L, Blanchet-Cohen A, Garnier D, Rak J, Lecuyer E. Comparative transcriptomic analysis of human and Drosophila extracellular vesicles. Sci Rep. 2016; 6:27680.doi: 10.1038/srep27680 [PubMed: 27282340]

Love MI, Huber W, Anders S. Moderated estimation of fold change and dispersion for RNA-seq data with DESeq2. Genome Biol. 2014; 15:550. [PubMed: 25516281]

Lyford GL, Yamagata K, Kaufmann WE, Barnes CA, Sanders LK, Copeland NG, Gilbert DJ, Jenkins NA, Lanahan AA, Worley PF. Arc, a growth factor and activity-regulated gene, encodes a novel cytoskeleton-associated protein that is enriched in neuronal dendrites. Neuron. 1995; 14:433–445. [PubMed: 7857651]

Mattaliano MD, Montana ES, Parisky KM, Littleton JT, Griffith LC. The Drosophila ARC homolog regulates behavioral responses to starvation. Molecular and cellular neurosciences. 2007; 36:211–221. [PubMed: 17707655]

Meckes DG Jr. Exosomal communication goes viral. J Virol. 2015; 89:5200–5203. [PubMed: 25740980]

Myrum C, Baumann A, Bustad HJ, Flydal MI, Mariaule V, Alvira S, Cuellar J, Haavik J, Soule J, Valpuesta JM, et al. Arc is a flexible modular protein capable of reversible self-oligomerization. Biochem J. 2015; 468:145–158. [PubMed: 25748042]

Nallamsetty S, Austin BP, Penrose KJ, Waugh DS. Gateway vectors for the production of combinatorially-tagged His6-MBP fusion proteins in the cytoplasm and periplasm of Escherichia coli. Protein Sci. 2005; 14:2964–2971. [PubMed: 16322578]

Nefedova L, Kim A. Mechanisms of LTR-Retroelement Transposition: Lessons from Drosophila melanogaster. Viruses. 2017; 9

Nishida KM, Miyoshi K, Ogino A, Miyoshi T, Siomi H, Siomi MC. Roles of R2D2, a cytoplasmic D2 body component, in the endogenous siRNA pathway in Drosophila. Mol Cell. 2013; 49:680–691. [PubMed: 23375501]

Peebles CL, Yoo J, Thwin MT, Palop JJ, Noebels JL, Finkbeiner S. Arc regulates spine morphology and maintains network stability in vivo. Proc Natl Acad Sci U S A. 2010; 107:18173–18178. doi: 18110.11073/pnas.1006546107. Epub 1006542010 Oct 1006546104. [PubMed: 20921410]

Port F, Bullock SL. Creating Heritable Mutations in Drosophila with CRISPR-Cas9. Methods Mol Biol. 2016; 1478:145–160. [PubMed: 27730579]

Roberts A, Pachter L. Streaming fragment assignment for real-time analysis of sequencing experiments. Nat Methods. 2013; 10:71–73. [PubMed: 23160280]

Satoh AK, O'Tousa JE, Ozaki K, Ready DF. Rab11 mediates post-Golgi trafficking of rhodopsin to the photosensitive apical membrane of Drosophila photoreceptors. Development. 2005; 132:1487–1497. [PubMed: 15728675]

Schneider I. Cell lines derived from late embryonic stages of Drosophila melanogaster. J Embryol Exp Morphol. 1972; 27:353–365. [PubMed: 4625067]

Shepherd JD, Bear MF. New views of Arc, a master regulator of synaptic plasticity. Nat Neurosci. 2011; 14:279–284. doi:210.1038/nn.2708. Epub 2011 Jan 1030. [PubMed: 21278731]

Speese SD, Ashley J, Jokhi V, Nunnari J, Barria R, Li Y, Ataman B, Koon A, Chang YT, Li Q, et al. Nuclear envelope budding enables large ribonucleoprotein particle export during synaptic Wnt signaling. Cell. 2012; 149:832–846. [PubMed: 22579286]

Stewart BA, Atwood HL, Renger JJ, Wang J, Wu CF. Improved stability of Drosophila larval neuromuscular preparations in haemolymph-like physiological solutions. J Comp Physiol A. 1994; 175:179–191. [PubMed: 8071894]

Trapnell C, Roberts A, Goff L, Pertea G, Kim D, Kelley DR, Pimentel H, Salzberg SL, Rinn JL, Pachter L. Differential gene and transcript expression analysis of RNA-seq experiments with TopHat and Cufflinks. Nat Protoc. 2012; 7:562–578. [PubMed: 22383036]

Viola H, Ballarini F, Martinez MC, Moncada D. The tagging and capture hypothesis from synapse to memory. Prog Mol Biol Transl Sci. 2014; 122:391–423. DOI: 10.1016/B1978-1010-1012-420170-420175.400013-420171 [PubMed: 24484708]

Vizcaino JA, Csordas A, del-Toro N, Dianes JA, Griss J, Lavidas I, Mayer G, Perez-Riverol Y, Reisinger F, Ternent T, et al. 2016 update of the PRIDE database and its related tools. Nucleic Acids Res. 2016; 44:D447–456. [PubMed: 26527722]

Zhang W, Wu J, Ward MD, Yang S, Chuang YA, Xiao M, Li R, Leahy DJ, Worley PF. Structural basis of arc binding to synaptic proteins: implications for cognitive disease. Neuron. 2015; 86:490–500. doi:410.1016/j.neuron.2015.1003.1030. Epub 2015 Apr 1019. [PubMed: 25864631]

Highlights

- *arc1* mRNA/protein traffic across synapses via exovesicles, requiring its 3′UTR
- dArc-protein Gag binds *darc1* mRNA, and the protein forms capsid-like structures
- Exovesicles contain GAG-protein and Gag-encoding-mRNA of the retrotransposon Copia
- Transfer of *darc1* protein and/or mRNA is required for synaptic plasticity

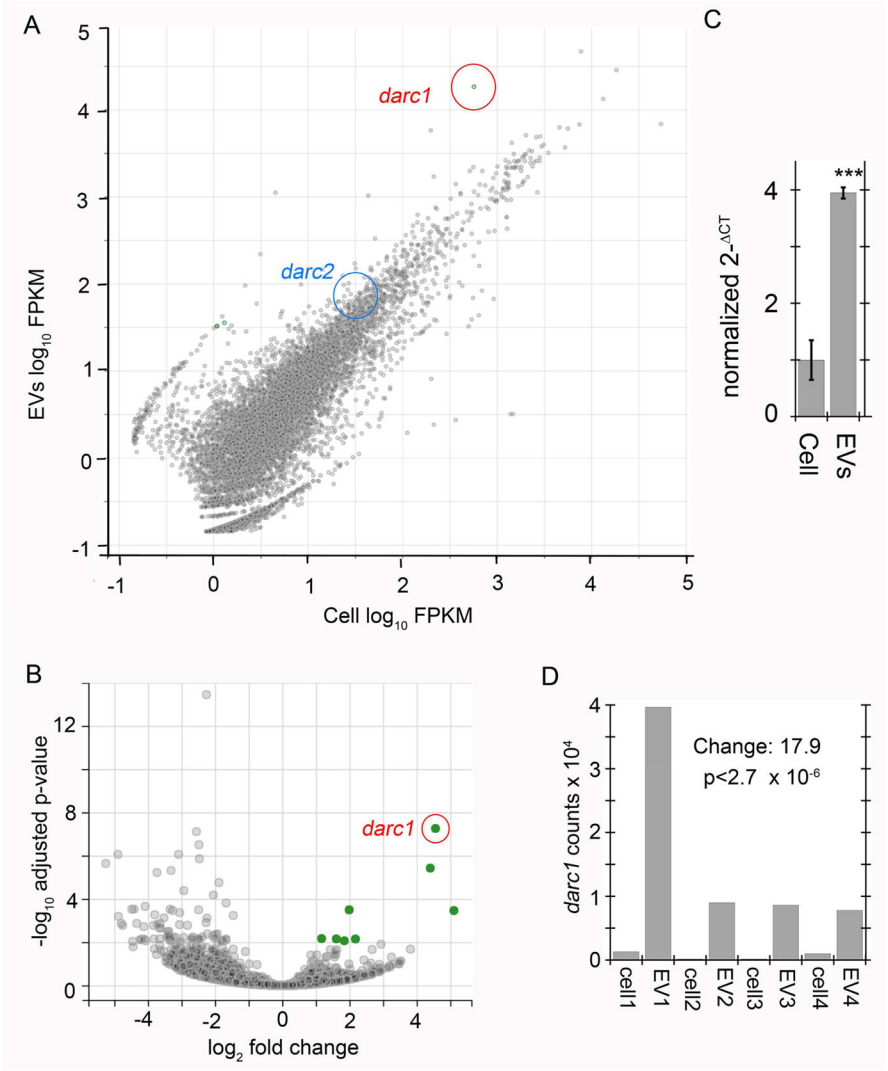

Figure 1. *darc1* mRNA is enriched in EVs

(**A**) Comparison of RNA expression levels in EV versus cellular RNA from S2 cells determined by deep sequencing, and enrichment of *darc1* (red) in the EV fraction. Note that *darc2* mRNA (blue) levels are not statistically different from cellular levels.

(**B**) Volcano Plot of RNA-Seq data from 4 replicates, where the x-axis represents fold change in transcripts from EVs vs. total cellular mRNA levels (a positive score represents enrichment, a negative score represents depletion). The y-axis represents statistical confidence for each x-axis point. Green circles are transcripts that are significantly enriched. *darc1* is encircled by a red marker.

(**C**) Normalized quantitative PCR confirming that *darc1* is enriched in the exosome fraction compared to the total cell. N= 3 biological replicates.

(**D**) Raw number of RNA-seq reads for *darc1* from 4 biological RNA-Seq replicates.

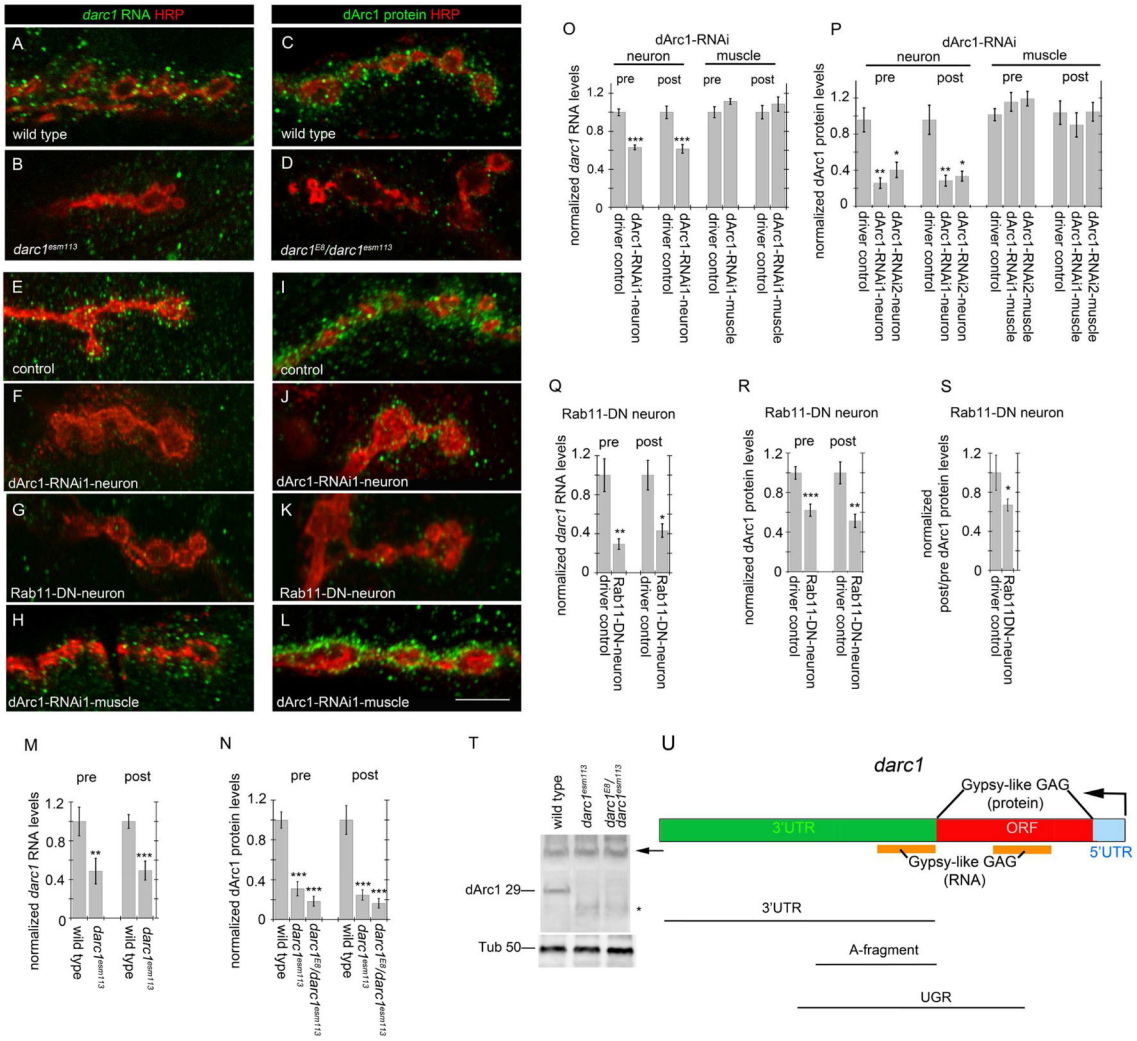

Figure 2. *darc1* mRNA and protein are present at the *Drosophila* NMJ, and are transferred from pre- to postsynaptic sites

(**A–D**) Confocal slices of NMJ branches in preparations double labeled with anti-HRP and either (**A,B**) a *darc1* FISH probe, or (**C,D**) anti-dArc1 in (**A**,**C**) wild type and (**B**) $darc1^{esm113}$ and (**D**) $darc1^{E8}/darc1^{esm113}$ mutants.

(**E–L**) Confocal slices of NMJ branches in preparations double labeled with anti-HRP and either (**E–H)** a *darc1* FISH probe, or (**I–L**) anti-dArc1, in (**E,I**) C380-Gal4/+ control, upon expression of (**F,J**) dArc1-RNAi-neuron (C380-Gal4>UAS-RNAi1), (**G,K**) Rab11-DN-neuron (C380-Gal4>UAS-Rab11DN), and (**H,L**) dArc1-RNAi1-muscle (C57-Gal4> dArc1-RNAi1).

(**M–R**) Quantification of (**M,O,Q**) normalized *darc1* FISH signal and (**N,P,R**) normalized dArc1 immunocytochemical signal at the NMJ in the indicated genotypes.

(**S**) Normalized ratio of postsynaptic to presynaptic signal in the indicated genotypes

(**T**) Western blot of body wall muscle protein extracts derived from the indicated genotypes probed sequentially with anti-dArc1 (top) and Tubulin (Tub; bottom). Numbers at the left of

the blots represent molecular weight in kilodaltons. Arrow points to an unspecific band labeled by the dArc1 antibody. Tub=tubulin.

(**U**) Diagram of *darc1* mRNA showing the 5′ UTR (blue), the open reading frame (ORF; red), and the 3′ UTR (green). Black lines underneath represent different portions of the *darc1* transcript. Orange bars represent regions of the *darc1* mRNA resembling Gypsy-like Gag sequences. Note that the entire ORF encodes a Gypsy-like Gag protein.

Calibration bar is 6 μm; N=(from left to right; animals/arbors) M(6/11, 6/10), N(12/16, 6/10, 6/10), O(8/14, 8/13, 8/15, 8/16), P(21/44, 12/24, 9/14, 18/29, 9/17, 9/14), Q(8/14, 8/13), R(15/28, 15/28), S(15/28,15/28); Data are represented as mean and error bars represent SEM; statistical analysis was conducted using student's t-test for M and one-way ANOVA with Tukey Post Hoc test for the rest of the graphs. *= $p < 0.05$; **= $p < 0.001$; ***= $p < 0.0001$.

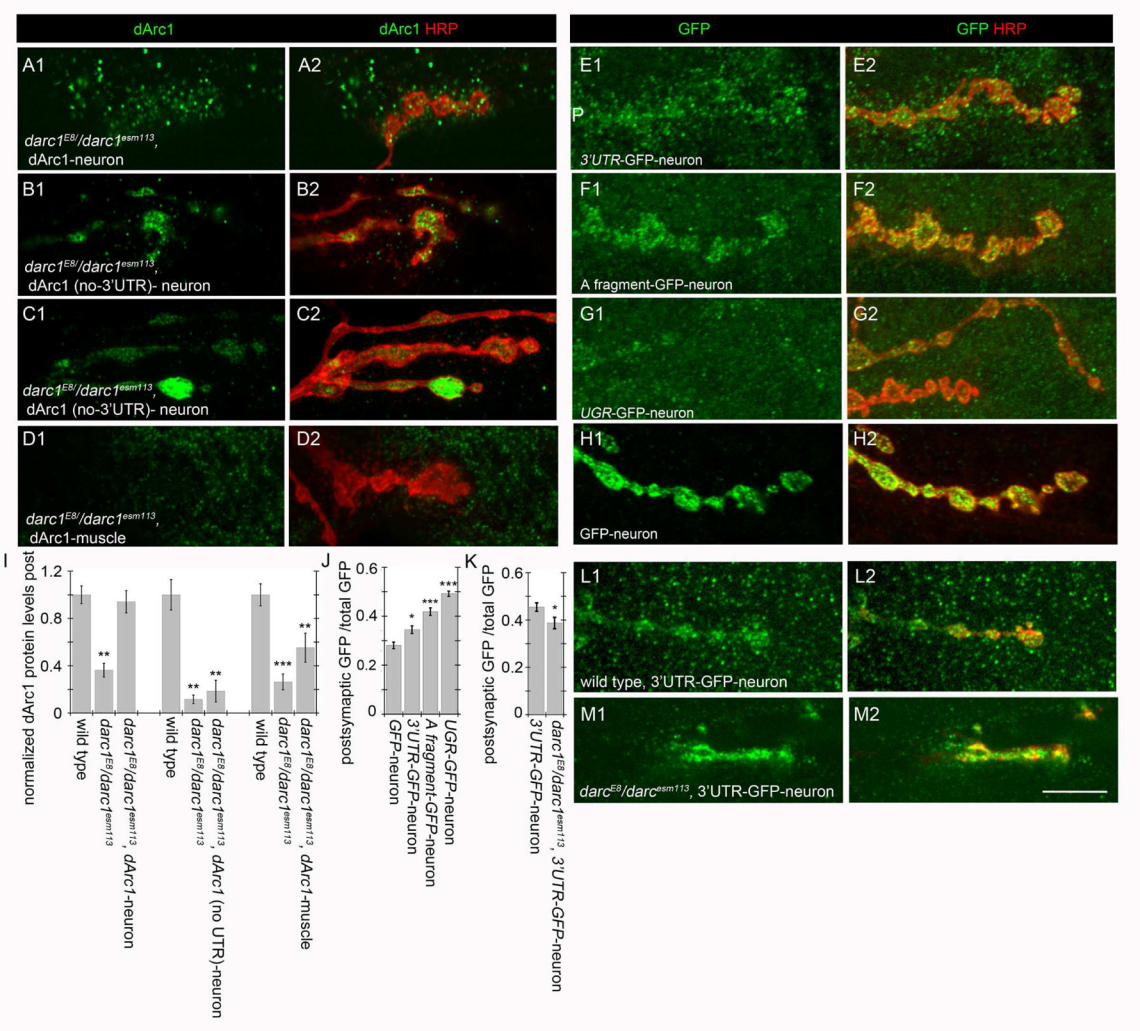

Figure 3. *darc1* mRNA and protein transfer across synaptic boutons depends on *darc1* 3′*UTR* (see also Supplemental Fig. 1)

(**A–H,L–M**) Single confocal slices of NMJ branches

(**A–D**) from *darc1* mutant larvae expressing dArc1 transgenes either (**A,D**) containing, or (**B,C**) lacking the 3′UTR, double labeled with antibodies to dArc1 and HRP. Transgenes were expressed in (**A–C**) neurons (C380-Gal4>transgene)or (**D**) muscles (C57-Gal4>transgene).

(**E**–**H**) in preparations double labeled with GFP and HRP from larvae expressing (**E**) *darc1* 3′UTR-GFP-neuron (C380> *darc1* 3′UTR-GFP), (**F**) *darc1* 3′UTR A-fragment-GFP-neuron (C380-Gal4> *darc1* 3′UTR A-fragment-GFP, (**G**) UGR-GFP (C380>UAS-UGR-GFP), (**H**) GFP neuron (C380-Gal4>UAS-GFP).

(**L,M**) in preparations double labeled with GFP and HRP from *darc1* 3′UTR-GFP-neuron (C380> *darc1* 3′UTR-GFP) in a (**L**) wild type and (**M**) $darc1^{E8}/darc1^{esm113}$ mutant background.

(**I**–**K**) Quantification of (**I**) dArc1 immunoreactive and (**J,K**) GFP immunoreactive signal in the indicated genotypes.

(**L**) Diagram of *darc1* mRNA showing the 5′ (blue), the ORF encoding (red), and 3′ (green) UTR. The black lines underneath represent different portions of the *darc1* transcript testing the *darc1* localization signal.

Calibration bar is 8 μm; N=(from left to right; animals/arbors) I(10/13, 10/13, 10/23, 9/17, 9/15, 9/13, 9/19, 9/17, 9/15), J(9/18, 15/27, 9/18, 9/16), K(10/29, 10/25). Data are represented as mean and error bars represent SEM; statistical analysis was conducted using one-way ANOVA with Tukey post hoc test for I,J, and Student's t-test for K. *= $p < 0.05$; **= $p < 0.001$; ***= $p < 0.0001$.

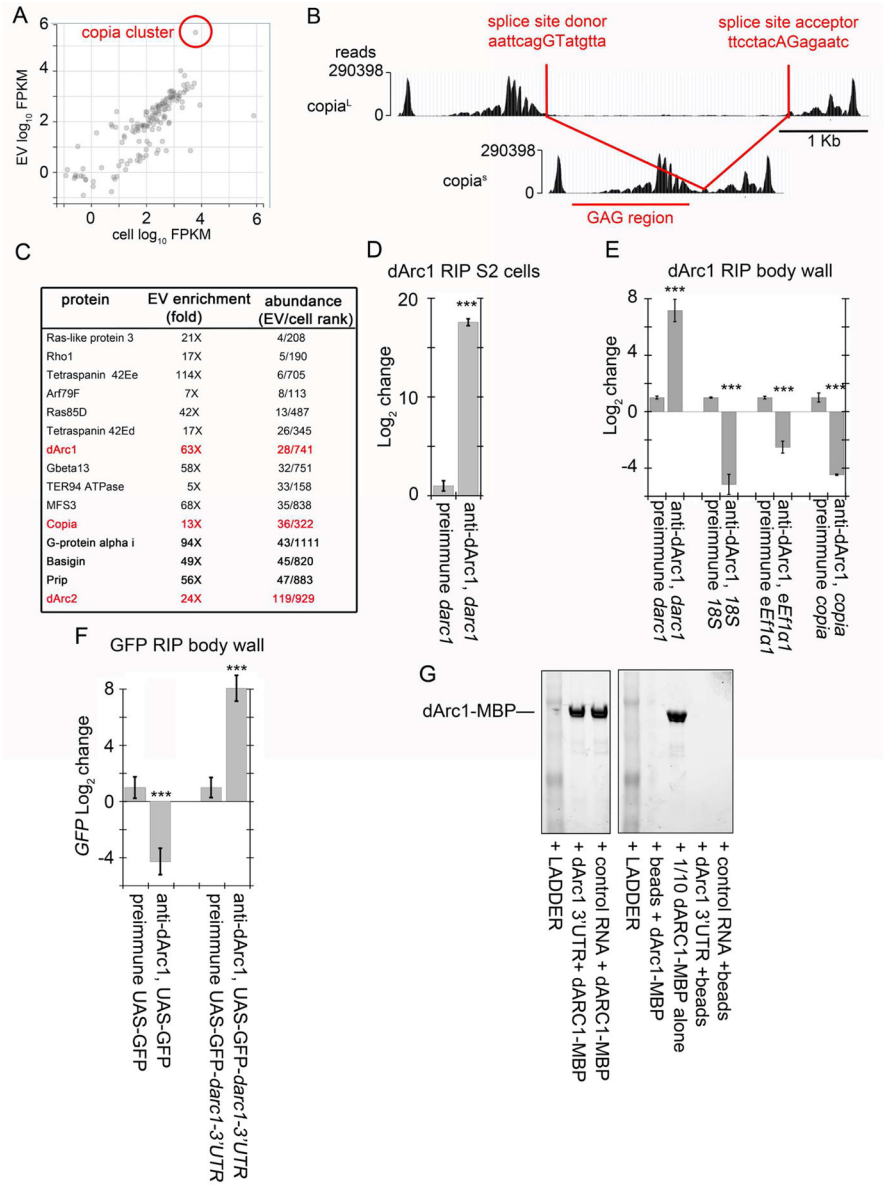

Figure 4. Enrichment of Copia-retrotransposon RNA and protein in S2 cell EVs and *darc1* mRNA association with*darc1* protein

(**A**) Enrichment of *copia* mRNA in the S2 EV fraction.

(**B**) Long (L) and short (S) *copia* isoforms, predicted to be generated by alternative RNA splicing, and enrichment of *copia*^{S}, encoding the Gag region, in EVs.

(**C**) Selected proteins showing enrichment in S2 cell EVs and their abundance in the EV vs cellular fractions, highlighting dArc1, dArc2 and Copia.

(**D,E**) Immunoprecipitation of *darc1* RNA using anti-dArc1 antibodies from extracts of (**D**) S2 cells and (**E**) body wall muscles.

(**F**) Immunoprecipitation of GFP RNA using anti-dArc1 antibodies from extracts of body wall muscles with neurons expressing either GFP alone or GFP upstream of the *darc1* 3′UTR.

(**G**) Biotinylated RNA pull down of dArc1, using biotinylated darc1 3′UTR RNA or control RNA. Both pull down dArc1 protein, while beads or RNA alone do not.

N=3 biological repeats for D,E,F; data are represented as mean and error bars represent SEM; statistical analysis was conducted using student's T-test; *= $p < 0.05$; **= $p < 0.001$; ***= $p < 0.0001$.

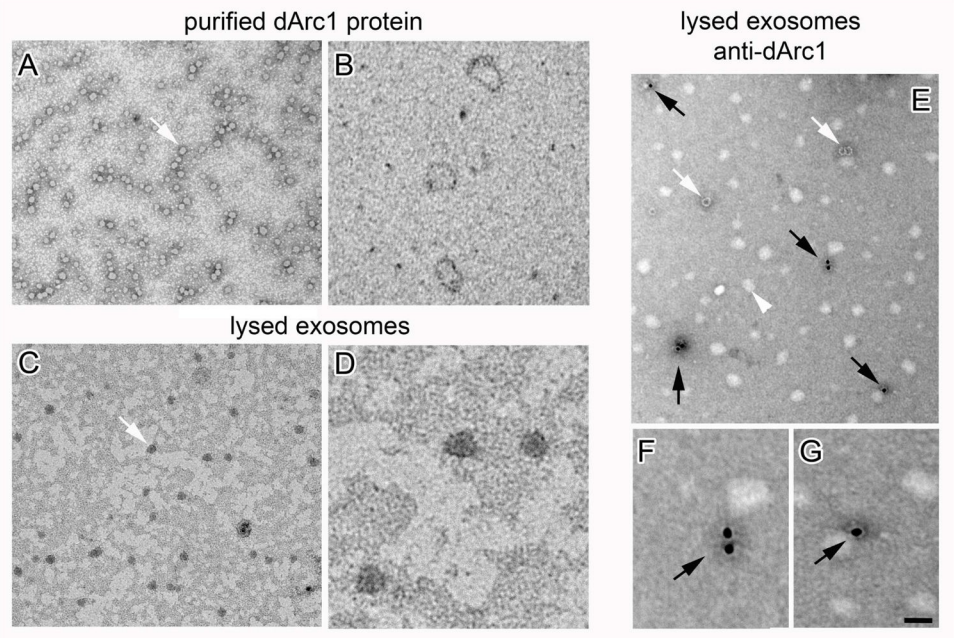

Figure 5. Purified *dArc1* protein assembles into capsid-like structures and these structures are contained in EVs

(**A,B**) Negatively stained capsid-like structures (white arrow) formed by purified dArc1 protein shown at (**A**) low and (**B**) high magnification.

(**C,D**) Capsid-like structures (white arrow) observed after EV lysis, shown at (**A**) low and (**B**) high magnification.

(**E–G**) Anti-dArc1 ImmunoEM labeling of capsid-like structures (black arrows) derived from lysed EVs, shown at (**E**) low and (**F,G**) high magnification. White arrows point to unlabeled capsid like structures. Calibration bar is 120 nm for A,C,E and 40 nm for B,D,F,G.

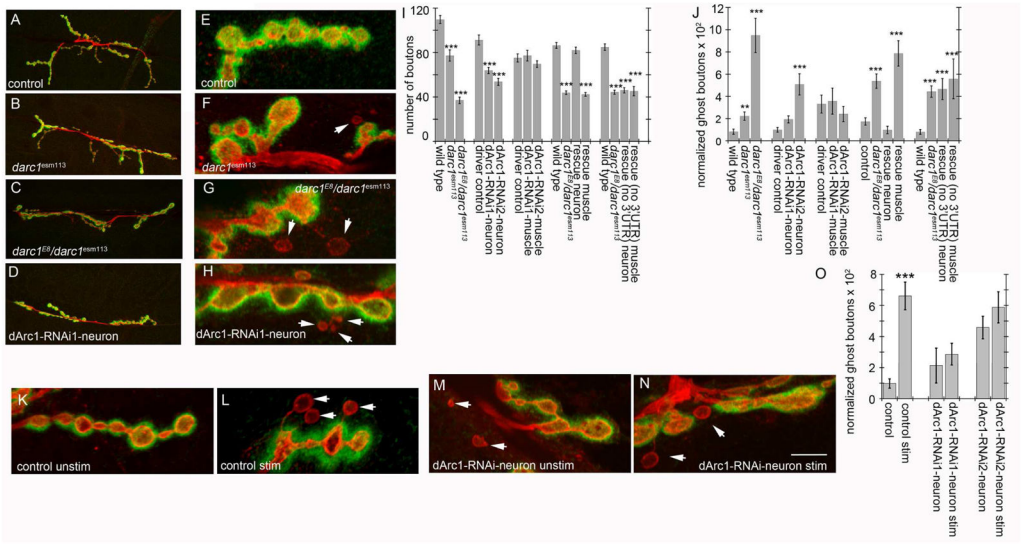

Figure 6. dArc1 influences developmental and activity-dependent plasticity at the NMJ

(**A–D**) Merged confocal Z-stacks of NMJ arbors labeled with antibodies against HRP and DLG in (**A**) C380-Gal4/+ control, (**B**) *darc1*^{esm113} mutant, (**C**) *darc1*^{E8}/*darc1*^{esm113} mutant, and (**D**) motorneuron expression of dArc1-RNAi1.

(**E–H**) High magnification view of single confocal slices through NMJ branches in the same genotypes as (**A–D**).

(**I,J,O**) Quantification of third instar larval (**I**) synaptic boutons, (**J**) ghost boutons, and (**O**) activity induced ghost boutons in the indicated genotypes and conditions.

(**K–M**) Single confocal slices of NMJs in preparations with antibodies against HRP and DLG in (**K,L**) unstimulated NMJs and (**M,N**) after stimulating NMJs with a spaced stimulation protocol in the indicated genotypes.

Calibration bar is 46 μm in **A**–**H** and 6 μm in **K–N**; N=(from left to right; animals/arbors) I,J(14/27, 8/15, 6/12, 6/12, 6/10, 6/12, 12/21, 6/12, 6/12, 12/21, 8/16, 6/10, 6/10, 14/27, 10/20, 9/16, 6/10), O(12/19,12/22,6/12,6/11,7/14,7/12). Data are represented as mean and error bars represent SEM. Statistical analysis was conducted using one-way ANOVA with Tukey post hoc test for I,J and Student's t-test for O. *= $p < 0.05$; **= $p < 0.001$; ***= $p < 0.0001$.

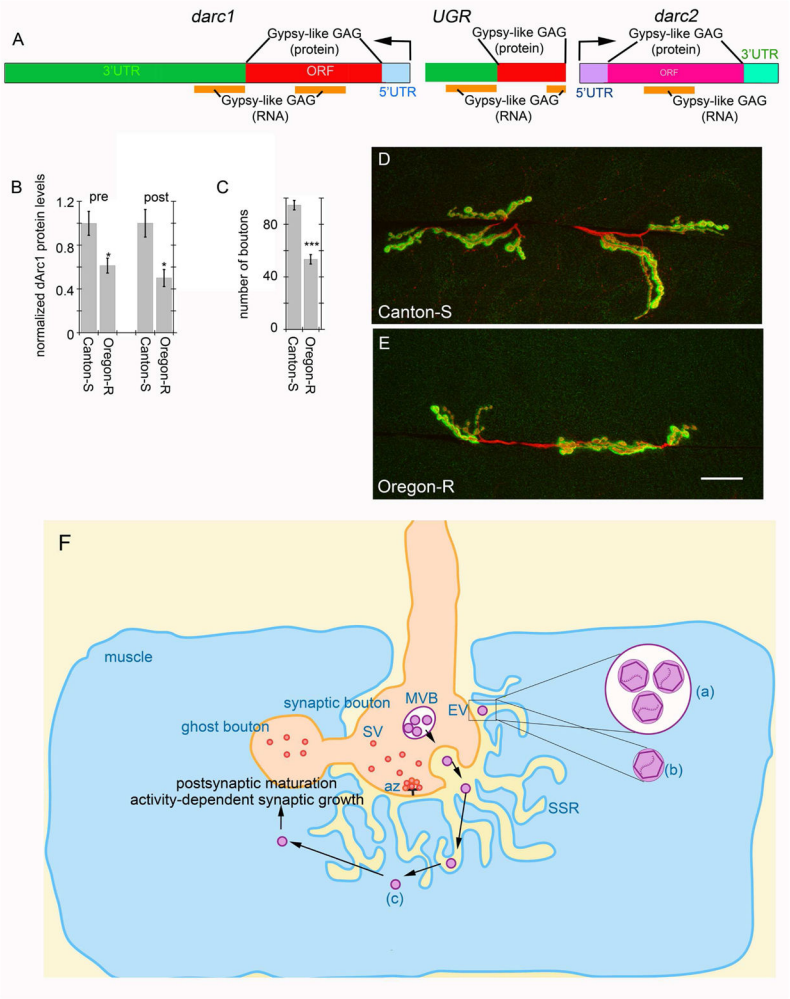

Figure 7. Consequences of the UGR for *darc1* expression and NMJ morphology, and proposed model of dArc1 transfer (see also Supplemental Fig. 2)

(**A**) Diagram of the darc1 genomic region in OR showing the UGR element between the *darc1* and *darc2* genes.

(**B,C**) Quantification in the indicated genotypes of (**B**) anti-dArc1 signal and (**C**) number of synaptic boutons.

(**D**,**E**) Merged confocal Z-stacks of NMJ arbors labeled with antibodies to HRP and DLG in (**D**) Canton-S and (**E**) Oregon-R.

(**F**) Diagram depicting a larval NMJ, in which exosome-like vesicles (EV) containing dArc1 protein and transcript are packaged then released from non-synaptic sites. It is still unclear whether these EVs contain multiple enveloped capsid-like particles (a) or a single capsid-like structure (b). These capsid-like particles (c) are taken up by the postsynaptic muscle, either through EV fusion with the muscle membrane, or endocytosis and further fusion with the endosome membrane. We propose that this transfer serves to stimulate synaptic maturation, as downregulation of presynaptic dArc1 leads to accumulation of ghost boutons. (MVB = multivesicular body, SV = synaptic vesicle, AZ = active zone, SSR = subsynaptic reticulum)

Calibration bar is 26 μm; N=(from left to right; animals/arbors) B(12/12,12/24), C(6/10,6/12); data are represented as mean and error bars represent SEM. Statistical analysis was conducted using student's T-test. *= $p < 0.05$; **= $p < 0.001$; ***= $p < 0.0001$.